




New chemical and mineralogical data on mosaics from the South aisle wall of Monreale Cathedral (Italy)

Alessia Coccato¹, Maria Cristina Caggiani^{1,a} , Claudio Finocchiaro¹, Maura Fugazzotto¹, Gabriele Lanzafame¹, Paolo Mazzoleni¹, Girolamo Nucatolo², Roberta Occhipinti¹, Silvia Starinieri², Antonio Stroschio¹, Germana Barone¹

¹ Department of Biological, Geological and Environmental Sciences, University of Catania, Corso Italia 57, 95128 Catania, Italy

² Piacenti S.p.a., Via Marradi 38, 59100 Prato, Italy

Received: 24 November 2022 / Accepted: 8 May 2023

© The Author(s) 2023

Abstract Due to the surprising lack of knowledge concerning raw materials and production technology employed to make mosaics after the twelfth century, an archaeometric investigation was carried out on the materials constituting the mosaic decoration of the South aisle wall of Monreale Cathedral (Italy), taking advantage of a conservation intervention. In this work, fallen coloured or gilded glass *tesserae* to be repositioned were studied by means of a combination of a molecular technique (Raman spectroscopy) and an elemental one (portable X-ray Fluorescence, pXRF); also, efflorescences affecting the general conservation state and samples of the respective bedding mortar were analysed with the former technique and with X-ray diffraction (XRD). The raw materials used and, consequently, the different compositions characterizing gilded vs. coloured glass *tesserae* were highlighted with the vibrational spectroscopy; chromophores and trace elements were detected by pXRF. This complementary approach allowed to disclose clues about glass-manufacturing technique and raw materials. The nature of the salts was also ascertained through Raman spectroscopy and XRD, for the benefit of the conservation procedure, and connected to the mortars' composition.

1 Introduction

The natural and artificial materials constituting historic mosaics, such as stone, glass and glass paste *tesserae* besides bedding mortars, are frequently studied from a chemical and mineralogical perspective. Decorative polychrome mosaics are found in Hellenistic, Roman, Paleo-Christian and Byzantine contexts, as well as in Islamic ones.

Monreale Cathedral (Sicily, Italy), built starting from 1172 by king William II “The Good”, reflects the unifying force of the Norman sovereign in its architectural design and decorative apparatus: the extensive gilded mosaic decoration, whose manufacture was concluded in the nineteenth century only, powerfully displays the balance achieved between Western, Byzantine and Arab-Islamic civilizations in Sicily [1]. The astonishing mosaic decoration (Fig. 1) comprises, in the lower level, a tall marble dado with mosaic-decorated pilasters and a geometric frieze running all along the perimeter of the Cathedral. The latter includes both gilded and coloured glass *tesserae* (blue, green, black and red) and white marble slabs of various shapes and dimensions, to create the form of palmettes (little palm trees). In the upper part of the walls and the apse vaults, figurative scenes are represented. Smaller stone and glass *tesserae*, more regular in their shape, allow to imitate skin tones and to reproduce shadows thanks to their richer polychromy. Finally, the gilded glass *tesserae* constituting the background strongly characterize this section of the decorative setup.

The raw materials, colourants and opacifiers employed to make glass, as well as the microstructure of the vitreous matrix, can convey information on manufacturing technology, which is related to production practices, which in turn can support provenance and chronological interpretations on the mosaics manufacture. Numerous examples of analytical investigations of glass *tesserae* from mosaics of different provenances and epochs can be found in literature [2–9], many of which concern the Roman age [2, 3, 7, 10]. Studies on palaeo-Christian and Byzantine mosaics combined chemical with molecular/mineralogical analyses: they involved for example St. Prosdocimus Church in Padova (Veneto, Italy), with glassy networks typical of Roman and Late Roman *tesserae* [6, 11–13], the Great Umayyad Mosque of Córdoba (Spain), characterized by high-boron glass composition [14] and early sixth century glass *tesserae* from *Villa di Teodorico* in Galeata (Northern Italy) [9]. In all cases, not only the expected different colouring agents were found, but also a variety of opacifying materials used within the same context. On the other hand, chemical and mineralogical data concerning mosaic materials after the twelfth century AD are rarer, the most famous example being fourteenth century samples from the Basilica of St. Marcus in Venice [15–17], for which some hypotheses were formulated concerning the probable first evidence of a Venetian production of mosaic *tesserae* [15, 16]. Concerning the composition of bedding mortars, the great part of the studies is focused on Roman examples such as [18–20], sometimes connected to conservation issues [21]; one of the few examples

^a e-mail: mariacristina.caggiani@unict.it (corresponding author)

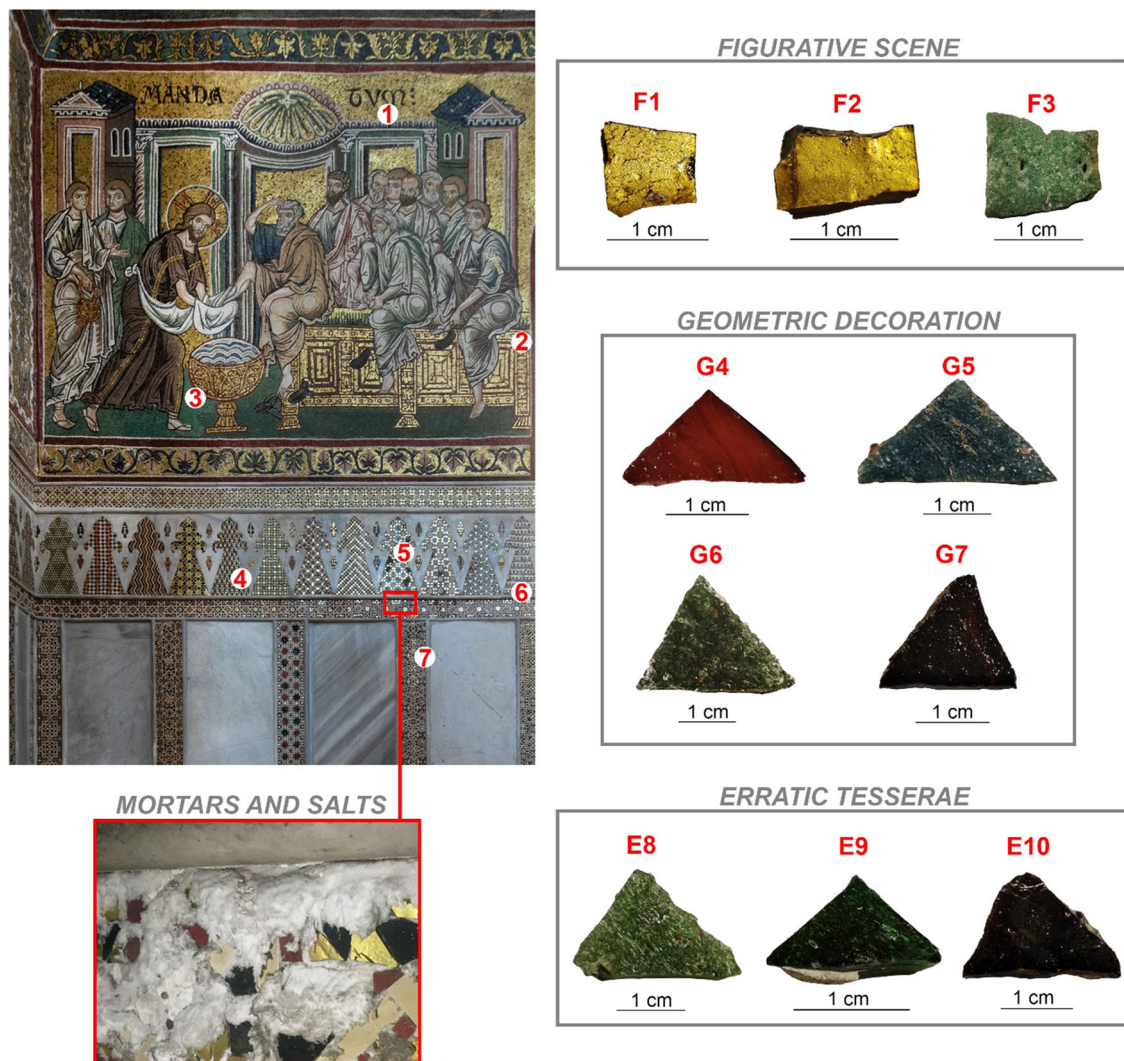


Fig. 1 Detail of the South aisle wall of Monreale Cathedral involved in the conservation site, with location and photographs of the sampled mortars and salts and of the fallen *tesserae*

regarding more recent case studies is the investigation of vaterite presence in mortars of a mosaic dated to the end of the sixteenth century in the Saint Peter Basilica, Vatican City [22].

Surprisingly enough, archaeometric investigations on Monreale mosaics appear to be limited to a SEM–EDS study of some production wastes coming from what has been interpreted as a deposit or service room for a twelfth–thirteenth centuries mosaic workshop [1] and to portable X-ray Fluorescence (pXRF) analyses of *tesserae* in the area of the portal [23].

The archaeometric investigation here carried out has been conducted as part of a conservation intervention on the South aisle wall [24]. The frame illustrating “The washing of the feet” and the corresponding section of the frieze with palmettes (Fig. 1) have recently been affected by water infiltrations, which caused salts efflorescence in the mortar and the subsequent detachment of some *tesserae*. This was included in the pilot restoration site of the project “Advanced Green Materials for Cultural Heritage (AGM for CuHe)” (PNR funded with code: ARS01_00697; CUP E66C18000380005), aimed at implementing new generation eco-friendly materials for the conservation of cultural heritage [24, 25 and references therein]. The instalment of the conservation site offered multiple research opportunities. First, it was possible to investigate the nature of the mortar and the efflorescences affecting it in view of the restoration campaign. Moreover, the analysis of the glass *tesserae* allowed to start to fill the gap in the literature concerning this important historical-artistic site. To assess the different chemical and mineralogical composition of the *tesserae*, non-destructive analyses were carried out taking advantage of the detached materials (Fig. 1): a well-established and successful approach for the study of glass, comprising a combination of pXRF and Raman spectroscopy [26–30] was applied in order to characterize coloured glass and to tackle the above-mentioned technological aspects. Though not allowing the better performances of some destructive techniques, the followed analytical protocol answered the need of re-allocating the *tesserae* in the mosaics within the end of the conservation intervention. The advantage of using a multi-analytical non-destructive approach was therefore exploited, at the same

time combining the benefits and drawbacks of the two complementary techniques. In detail, information about the characteristic chromophores and about the glass composition could be obtained by elemental pXRF analysis, while the study of the glass network and the detection of the crystalline compounds were possible thanks to molecular vibrational spectroscopy. Raman spectroscopy and XRD were also useful for the definition of the mineralogical composition of mortars and salts.

2 Materials and methods

2.1 Samples

A set of 10 *tesserae* waiting for reintegration was studied: 3 green (G6, E8, E9), 2 gilded (F1, F2), 2 black (G7, E10), 1 blue (G5), 1 turquoise (F3) and 1 red (G4) (Fig. 1). Both the G4 and G7 *tesserae* have a banded aspect, respectively in different shades of red and with reddish areas within the black. *Tesserae* from the geometric decorations, as well as the erratic ones, are triangular, while those from the figurative scene (the gilded and the turquoise ones) are rectangular; they range between 7 and 32 mm in width and between 4 and 7 mm in thickness. The *cartellina* of *tesserae* F1 and F2 is 0.3–0.4 mm thick. *Tesserae* were cleaned with water to remove any residual dust. For pXRF, the analyses were carried out on the outer surface of the coloured glass *tesserae*, while the gilded ones were measured on both sides. For Raman spectroscopy, the analyses were carried out on the thickness of the *tesserae*, in order to avoid superficial alteration. Samples of the mortar and the respective efflorescences were also considered. See Fig. 1 for a detailed mapping of the materials provenance.

The Corning Archaeological Reference Glasses A, B and D [31] (Smithsonian Microbeam Standards: respectively NMNM 117,218–4, NMNM 117,218–1 and NMNM 117,218–3) were also analysed as references.

2.2 Techniques

For micro-Raman investigation, a Jasco NRS3100 spectrometer equipped with $50\times$ LWD and $100\times$ microscope objectives was used, reaching minimum lateral and depth resolutions as low as $1\ \mu\text{m}$ by means of a confocal hole. For the glass analysis, the 532 nm laser was used with power ranging between 2.5 and 7 mW, in combination with a 1800 gr/mm dispersing system (spectral resolution of ca. $1\ \text{cm}^{-1}$), a Notch filter and a Peltier-cooled ($-55\ ^\circ\text{C}$) 1024×128 CCD. For the mortars and salts analysis, the 785 nm laser with a power of about 10 mW in combination with a 1800 gr/mm grating was used for the $200\text{--}1200\ \text{cm}^{-1}$ region analysis (spectral resolution better than $3\ \text{cm}^{-1}$), while the 532 nm laser with a power of about 3.5 mW combined with the 600 gr/mm grating was employed for the $2500\text{--}4000\ \text{cm}^{-1}$ range (spectral resolution of ca. $5\ \text{cm}^{-1}$). The system was calibrated using the $520.7\ \text{cm}^{-1}$ Raman band of silicon before each experimental session. Baseline subtraction and spectral decomposition were obtained with LabSpec software: the former was carried out following a well-established procedure for glass study [30, 32, 33], the latter using Gauss-Lorentz curves, with the aim of calculating the areas of the glass-connected bands excluding the contribution of crystalline phases.

pXRF analyses were performed in air with a Bruker Elio system equipped with a Rh target X-ray tube and a Silicon Drift Detector. Spectra were acquired over 180 s (live time) with 40 kV and $80\ \mu\text{A}$, with no filter. PyMCA [34] was used for the qualitative and semi-quantitative interpretation of the spectra. Although the information on the glass-forming elements cannot be fully understood with this analytical technique, its non-destructiveness and the simultaneous measurement of trace elements make it a powerful tool in the analysis of cultural heritage glass artefacts [35]. A comparison has been performed between the certified and the experimental concentrations of selected elements, by taking into account the limited capability of pXRF to detect light elements. The first were retrieved from [31] and recalculated excluding elements not detectable with pXRF (Table 1), the latter were obtained using PyMCA and an adapted configuration file for the instrument, analytical parameters and matrix. For comparison purposes of standard glass references with the *tesserae* by pXRF, a recalculation to 100% of the certified values of Corning glasses was performed (Table 1) after discarding the contribution of sodium, magnesium and aluminium from the overall composition of glass reported in [31]. Linear correlations are shown for SiO_2 , K_2O , CaO , MnO , Fe_2O_3 , Co , Ni , Cu , Rb , Sr which allowed to establish calibration curves ($R > 0.95$ for all considered elements; for Rb only values of Corning glass A and D were considered) for correcting the semi-quantification of the *tesserae*. On the other hand, quantification could not be achieved for other elements, such as Sb and Pb, for which only a qualitative assessment will be provided based on the presence of their L-lines (Online Resource 1).

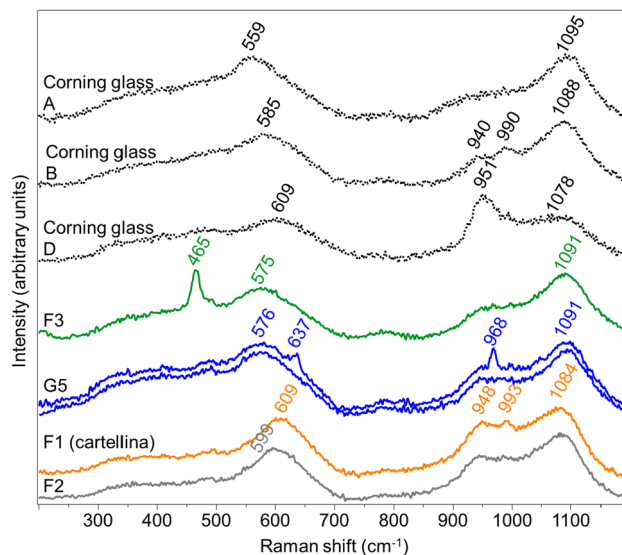
Mineralogical investigation was carried out using a Siemens D5000 diffractometer. The instrumental parameters were: Cu-K α radiation; Ni filter; 2θ angle $5\text{--}60^\circ$, angular step of 0.02° 2θ ; step time 2 s; divergence and anti-scatter slits of 1° and receiving slit of 0.1 mm. High Score Plus software v.4.8 was used for the qualitative interpretation of XRD data.

Table 1 Recalculated concentrations (wt% and ppm) of Corning glasses A, B and D without the lighter elements

	SiO ₂ (%)	K ₂ O (%)	CaO (%)	MnO (%)	Fe ₂ O ₃ (%)	Co (ppm)	Ni (ppm)	Cu (%)	Rb (ppm)	Sr (ppm)
<i>Corning A cert</i>	85.23	3.67	6.44	1.28	1.40	2177	256	1.50	128	1280
<i>Corning B cert</i>	81.91	1.33	11.39	0.33	0.45	612	1317	3.54	n.d	253
<i>Corning D cert</i>	66.42	13.59	17.80	0.66	0.63	277	601	0.46	60	685
Corning A*	85.25	3.70	6.34	1.33	1.42	2210	397	1.54	132	1338
Corning B*	82.26	1.35	11.70	0.41	0.55	666	1310	3.48	n.d	347
Corning D*	67.00	13.67	17.64	0.57	0.53	229	463	0.45	55	562
A cert—quant	− 0.02	− 0.03	0.10	− 0.05	− 0.03	− 33	− 141	− 0.04	− 4	− 58
B cert—quant	− 0.36	− 0.02	− 0.31	− 0.08	− 0.10	− 54	8	0.06	−	− 94
D cert—quant	− 0.58	− 0.09	0.15	0.10	0.10	47	138	0.01	5	124

Rows in italic (“cert”) are obtained by recalculating the certified values to the total of the elements selected for this study from [31]. Rows in bold (*) represent the obtained values from quantification in PyMCA with an adapted configuration file that includes only the elements selected for this study, and successive calibration. Finally, the absolute difference between the recalculated certified values (“cert”) and the results of PyMCA-based quantification (“quant”) is given. N.d. = not detected

Fig. 2 Representative baseline-subtracted Raman spectra of glasses. Top to bottom: Corning glasses A, B and D; samples F3, G5, F1 (*cartellina*), F2. Spectra are stacked for clarity



3 Results

3.1 Glassy network

As expected, all the Raman spectra show the typical broad bands of glass (Fig. 2).

The spectra were subjected to baseline correction (linear segments with fixed wavenumber ranges) and a band fitting procedure, following Colombari [30, 32, 33]. The so-called polymerization index, I_p , defined as the ratio between the bending and stretching areas, A_{500}/A_{1000} has been calculated for all the studied *tessere*, only considering the glass-related bands (centred, respectively, at 550–610 and 750–1100 cm^{-1}). Based on the I_p (Fig. 3), it appears that the transparent glass of the gilded *tessere* ($I_p \approx 1$) has a lower value compared to the coloured glasses, where it ranges between 1.2 and 1.4. All three Corning glasses show relatively low I_p values (between 0.85 and 1.15) and show a greater similarity with the transparent glass of *tessere* F1 and F2. On average, the I_p values of the erratic *tessere* are slightly increased compared to those of same colour and known provenance.

When plotting the position of the maximum of the stretching and of the bending bands (Fig. 4), the coloured glasses show very close positions for the stretching maxima and a higher variability for the bending ones. This group extends between Corning glass A and B. Overlaying our plot on that reporting a classification by Colombari and co-authors [36], it can be observed that all of them fall in, or close to, the soda-lime field, not allowing to distinguish possible mixed-alkali glasses.

The colourless glass, however, appears again clearly separated towards concentrations richer in calcium according to the reference diagram. The shift is mainly based on the bending maximum, which is higher and closer to that of Corning glass D, whose chemical composition is in good agreement with what obtained from vibrational spectroscopy. The stretching maximum of the colourless

Fig. 3 Polymerization index calculated for spectra acquired on different spots of the glass *tesserae* and Corning glasses A, B and D

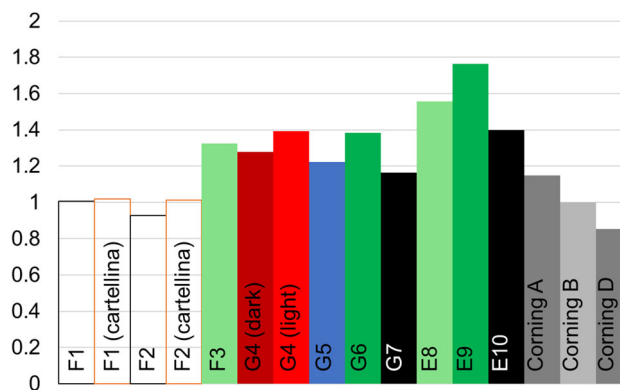
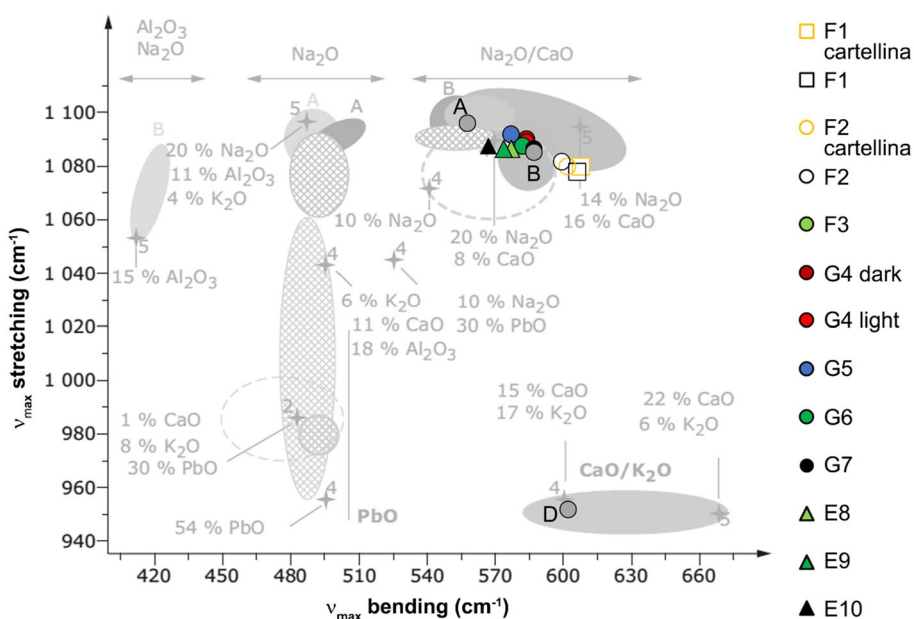


Fig. 4 Plot of the maxima of the bending and stretching observed in the glass *tesserae* (see legend) and in the Corning glasses A, B and D indicated with grey full symbols, overlaid on the differentiation guide proposed by Colombari in [36]



glass is slightly lower than for the other glasses, around 1080 cm^{-1} , corresponding to highly polymerized SiO_4^{4-} units (also known as Q^3 units, meaning 3 of the 4 oxygens are bound to another Si atom), while in Corning glass D, the maximum is at ca. 950 cm^{-1} , corresponding to Q^1 units instead (only one of the 4 oxygens is bound to another Si atom) [37, 38]. Moreover, the contribution at ca 780 cm^{-1} , assigned in literature to non-polymerized tetrahedra within a glass structure [37, 38], is extremely weak or even missing in the colourless glass spectra, suggesting a different connectivity of the glass network with respect to that of the coloured ones [32]. Compared to the thick glass, the Raman spectra on the *cartellina*, additionally, show the appearance of a band around 990 cm^{-1} . [1] describes the production process of these *tesserae*, which requires a double firing, in addition to the annealing phase. These multiple heating phases probably affect the glassy network and the configuration of the silicate units, favouring the polymerization process and therefore the increase of silicate chains and the disappearance of the less-polymerized units, as observed in glass fibres manufacturing [39].

Further compositional observations can be drawn from Raman spectral parameters, as for example by considering the I_p value and maximum of the Si–O stretching [40]. Here, the transparent glass of *tesserae* F1 and F2 groups together in the soda glass area, and all the coloured *tesserae* are identified as mixed alkali.

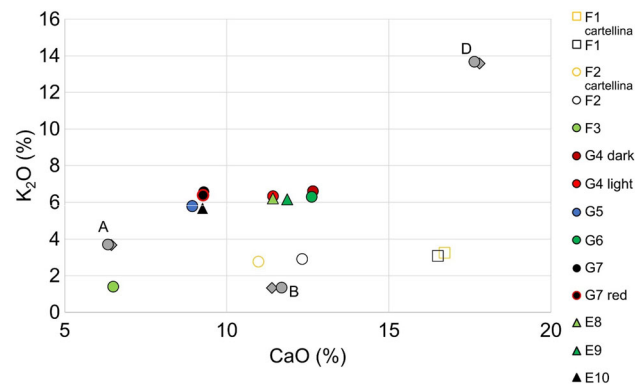
Although partial, pXRF data on some of the glass-forming elements (Table 2, Fig. 5) can help in further understand recipes and technologies. K_2O and CaO contents of the glasses appear to be intermediate between the ancient soda-lime glasses made with natron and plant ash (Corning A and B) and the Medieval European recipe (Corning D). However, the transparent glass and glass F3 have consistently lower potash contents, possibly indicating a different choice of fluxing ingredients and suggesting the use of natron, as exemplified in the reference glasses. These glasses also show low lead content, which appears as signals just above the noise level in both F2 and F3, and not detectable in F1 (Online Resource 1). Finally, when comparing CaO and K_2O of coloured glass, the blue and black *tesserae* group together, separate from the red and green shades. These glasses appear intermediate between

Table 2 Calculated concentrations (wt% and ppm) data obtained from quantification in PyMCA with an adapted configuration file including the elements selected for this study, and successive calibration based on Corning glass reference samples

	SiO ₂ (%)	K ₂ O (%)	CaO (%)	MnO (%)	Fe ₂ O ₃ (%)	Co (ppm)	Ni (ppm)	Cu (%)	Rb (ppm)	Sr (ppm)
F1 (<i>cartellina</i>)	76.35	3.26	16.72	1.42	1.85	188	132	0.25	91	1004
F1	76.83	3.09	16.52	1.35	1.78	165	121	0.33	28	824
F2 (<i>cartellina</i>)	81.95	2.77	10.98	2.03	1.85	78	95	0.31	59	835
F2	80.28	2.91	12.33	2.15	1.89	194	103	0.33	25	744
F3	89.92	1.40	6.50	0.17	1.05	70	63	0.88	19	725
G4 (dark)	75.26	6.60	12.66	0.67	2.42	149	139	2.30	24	540
G4 (light)	76.48	6.33	11.43	0.63	2.45	138	3867	2.21	31	583
G5	83.34	5.79	8.94	0.67	0.88	241	133	0.28	32	541
G6	76.91	6.28	12.62	0.70	1.09	97	122	2.29	52	743
G7	78.40	6.57	9.29	3.04	2.34	147	81	0.27	29	574
G7 (red)	78.75	6.37	9.27	2.52	2.50	154	71	0.47	50	708
E8	78.82	6.20	11.42	0.69	0.95	128	130	1.81	48	703
E9	76.46	6.16	11.87	0.70	1.11	159	159	3.58	24	635
E10	81.88	5.69	9.26	1.18	1.68	189	49	0.24	22	423

N.d. = not detected

Fig. 5 Bivariate diagram of the detected glass-forming elements potassium and calcium as oxides (wt%) in the studied *tesserae* (see legend) and Corning glasses A, B and D indicated with grey full symbols (circles represent the measured values, diamonds the certified ones after recalculation)



Corning glasses A and D, the latter being potash-rich. On the other hand, sample F3 is showing similarities with the transparent glass. The former moreover shows an enrichment in silicon-containing compounds, which likely affects the quantification results for this glass (see Paragraph 3.2).

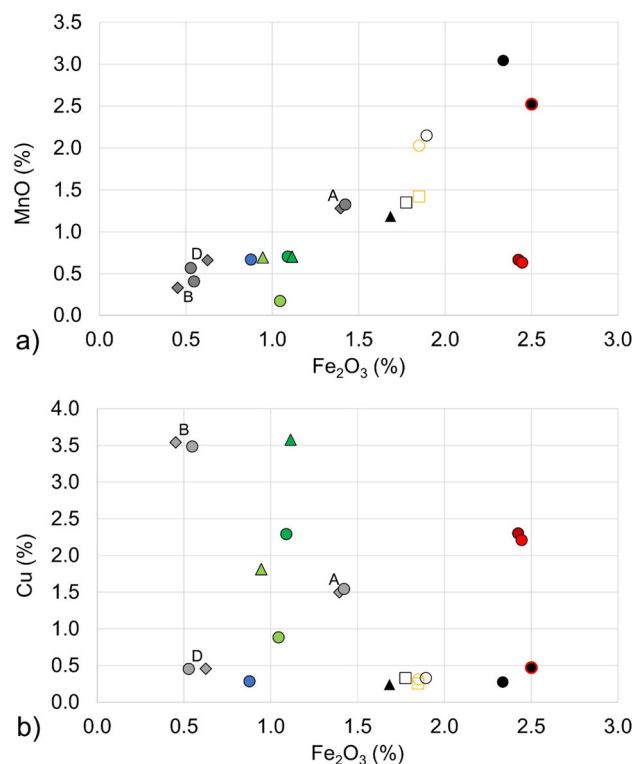
When considering strontium (Table 2), easily detected by pXRF, F3 and the thick glass of the gilded *tesserae* (F1, F2) are enriched in Sr compared to the other colours and to the *cartellina*. It is interesting to note that these values distinguish the *tesserae* from the figurative scene from those of the geometric decoration. In the literature, it has been reported that strontium in glass (both as absolute content and as isotopic distribution) can provide interesting insights into the used raw materials, suggesting that high contents are related to the use of marine biogenic sediments (e.g. shells), while strontium is practically absent from limestone [41, 42].

3.2 Crystalline compounds

The sharper signals obtained by means of Raman spectroscopy (Fig. 2), superimposed on the broader glass-related bands, are attributed to crystalline phases. In detail, they have been interpreted as quartz (SiO₂; 465 cm⁻¹), mostly present in the opaque turquoise *tessera* (F3) and wollastonite (Ca₃(Si₃O₉)) in the blue one (G5) (412, 637, 968 cm⁻¹) [43]. Quartz therefore contributes to the Si enrichment observed in pXRF analyses on the turquoise glass (F3), possibly in combination with selective leaching of alkalis [44]. These compounds have already been detected in archaeological glasses [1, 11, 43, 45] and particularly in Monreale green, blue and purple glass *tesserae* [1].

Quartz has been identified as opacifier in mosaic *tesserae* from Collesalveti (central Italy) and Carthage (Tunisia, second–third century AD) [5], from the Church of Saints Cosma and Damian in Rome (sixth century AD), from Messina, Sicily (probably thirteenth–sixteenth century) [45], as well as from basilica of St. Marcus in Venice (fourteenth century AD) [15, 16] and from Monreale, in the latter case associated with numerous bubbles [1]. The use of this poorly opacifying material seems to be connected

Fig. 6 Bivariate diagram of manganese vs. iron (a) and copper vs. iron (b) content in the studied *tesserae* (see Fig. 5 for legend) and Corning glasses A, B and D indicated with grey full symbols (circles represent the measured values, diamonds the certified ones after recalculation)



with the transition from antimony-opacified glass of Roman tradition to tin-based compounds in use since the Middle Ages and possible difficulties in accessing the relevant ores, or in mastering the recipes [1]. No antimony-containing compounds could be revealed, as expected from the pXRF results, that only detect Sb in the Corning glasses (Online Resource 1).

On the other hand, wollastonite seems to be linked to devitrification processes of soda-lime-silica glasses, such as the palaeo-Christian ones in Padua, Veneto [6]. It has also been interpreted in this sense in Monreale [1]. Wollastonite has also been observed in Padua, Veneto (Italy) and Tyana (Turkey) late-Antique glass *tesserae* [46] as a by-product of the use of bone powder as opacifier: the heating causes a reaction between hydroxylapatite ($\text{Ca}_5(\text{PO}_4)_3(\text{OH})$) and the glassy matrix, with the consequent formation of wollastonite; this process has also been verified with replicas of Byzantine glass [43].

It must be observed that neither antimony-based compounds nor cassiterite (SnO_2) were revealed, in agreement with pXRF data. These former were commonly used since the Roman imperial age, while the latter together with calcium phosphate were attested from Late Antiquity [9].

3.3 Chromophores

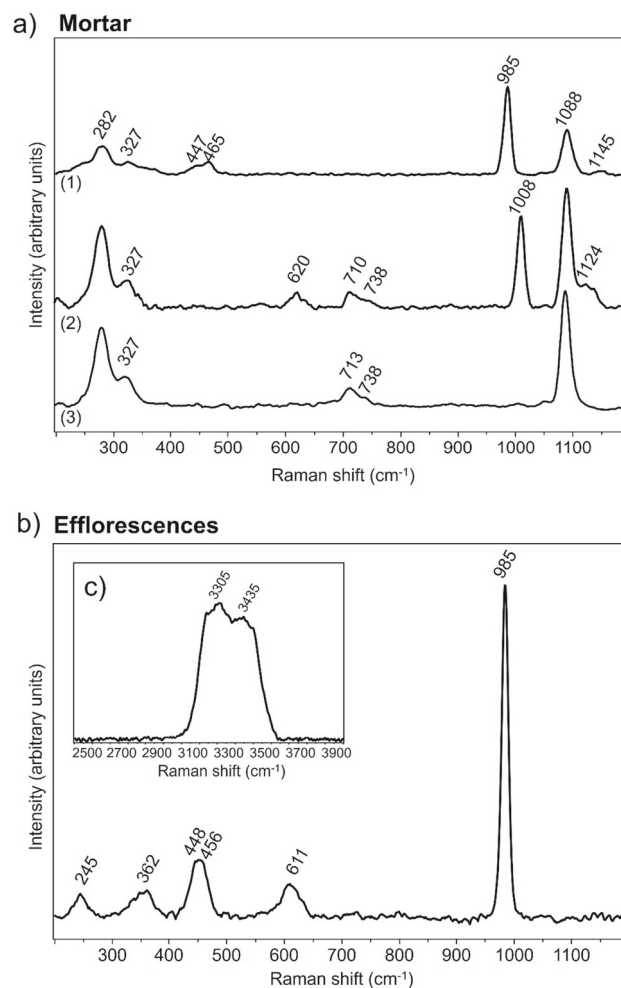
As well known, ionic chromophores and decolourants present in glass matrices cannot be detected by means of Raman spectroscopy [47, 48]; therefore, they were investigated by means of pXRF and the results are shown in Table 2.

When plotting the contents of manganese and iron, a general linear trend can be observed throughout the studied samples and references (Fig. 6a). Appropriate proportions of the two, combined with the correct redox conditions, yield a colourless glass [49, 50]. A detailed observation, however, allows to group together blue and green hues, with F3 having iron only; the two transparent glasses of F2 show an enrichment in manganese compared to the other gilded *tessera* F1. The erratic black *tessera* (E10) groups with these latter, confirming the inseparable contribution of iron and manganese as well as of the redox atmosphere to the final colour. *Tessera* G7 has the highest content of both elements, while high iron and low manganese are observed in the red *tessera* G4. The analysis carried out on a reddish spot in the black glass G7 has intermediate composition between red and black.

Copper content allows further differentiation (Fig. 6b): when it is associated with low amounts of iron, it imparts a greenish shade, whose highest intensity is observed in the dark green erratic *tessera* [1, 23]. Copper appears also associated with iron in the G4 red *tessera* [51], with little variations across the lighter and darker shades. It is absent in the black and transparent glasses, where iron is associated with manganese (Fig. 6a). Corning glass A and B have a bluish hue, and their copper content supports that.

The highest level of cobalt is observed in the blue *tessera* G5 (ca. 250 ppm). This might be sufficient to impart the blue colour to glass, together with ca. 0.3% of copper. Genuine gold is detected through the *cartellina* in both *tesserae* F1 and F2 (Online Resource 1).

Fig. 7 Representative baseline-subtracted 785-nm-laser Raman spectra of mortar samples (a) and a representative one acquired on salts (b). In the inset (c), a representative high wavenumber Raman spectrum acquired on the salts with 532 nm laser. Spectra are stacked for clarity



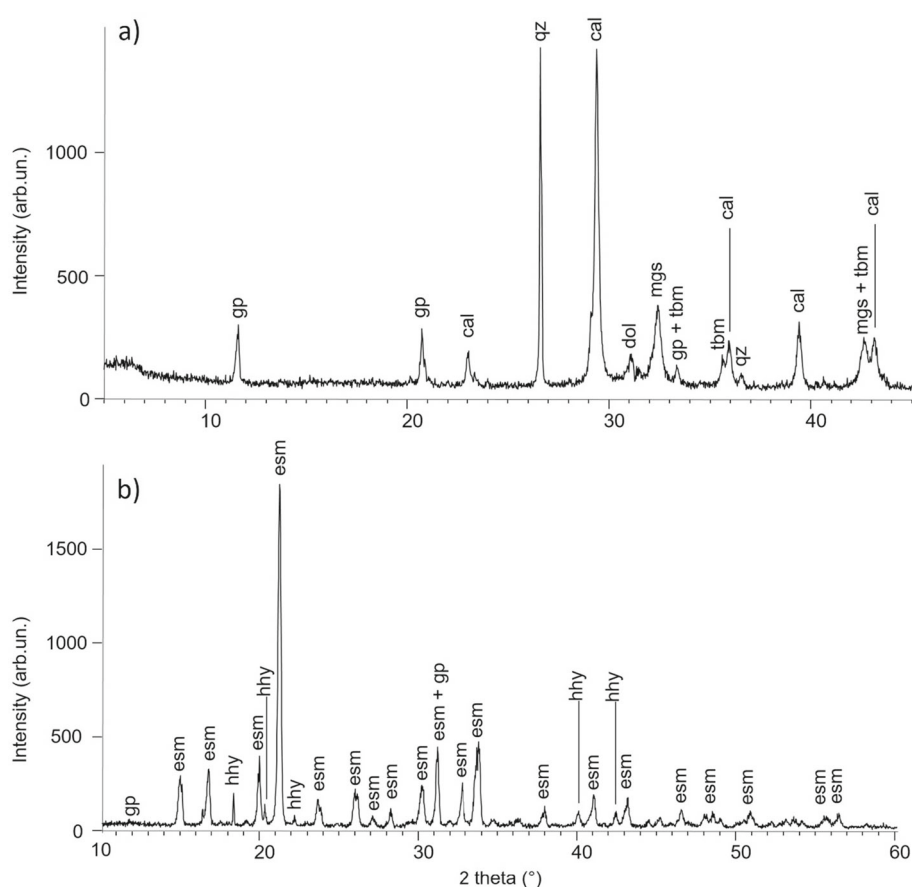
3.4 Mortars and salts

Several Raman point analyses were performed with 785 nm laser on samples scraped from the mortar, three representative spectra are shown in Fig. 7a. Different minerals were found; the carbonate phase shows a broadened ν_1 band around 1088 cm^{-1} : this might be due to the coexistence of calcite (CaCO_3 ; 282 , 710 and 1086 cm^{-1}) and magnesite (MgCO_3 ; 213 , 327 , 738 and 1090 cm^{-1}), the latter better distinguished by the 327 and 738 cm^{-1} bands [52]. Besides, it is well known that increasing amounts of magnesium in Mg-calcite shift the main band position towards higher wavenumbers; therefore, its possible presence should be considered, too [52]. Gypsum ($\text{CaSO}_4 \cdot 2\text{H}_2\text{O}$; 419 , 494 , 620 and 1008 cm^{-1}) and a hydrated magnesium sulphate (245 , 362 , 445 , 465 , 611 and 985 cm^{-1}) like epsomite ($\text{MgSO}_4 \cdot 7\text{H}_2\text{O}$) or hexahydrate ($\text{MgSO}_4 \cdot 6\text{H}_2\text{O}$) [53, 54] could also be found.

The Raman spectra acquired on the efflorescences can all be represented by the spectrum in Fig. 7b, where the above-mentioned signals of hydrated magnesium sulphate are visible, mirroring the magnesian nature of the mortar. Figure 7c shows a representative Raman spectrum of salts acquired with the green laser in the $2500\text{--}4000\text{ cm}^{-1}$ region, which could help in the distinction of magnesium sulphates at different hydration levels. The shape of the band and the position of the maxima at about 3305 and 3435 cm^{-1} lead to the identification of epsomite [55]. XRD measurements were conducted on representative samples of both mortars and salts. The mineralogical composition of the mortar in Fig. 8a is determined by the presence of calcite, magnesite, gypsum, quartz, dolomite ($\text{CaMg}(\text{CO}_3)_2$) and CSH (calcium silicate hydrates, e.g. tobermorite) phases, while the salts sample (Fig. 8b) shows the presence of gypsum and both epsomite and hexahydrate, which was not identified with Raman spectroscopy. This apparent discrepancy in results should be attributed to the different sampled volume between the two techniques.

Mortars sulphation with the consequent crystallization of magnesium sulphate and gypsum is common whenever combining a magnesium-rich mortar and a sulphate-bearing compound [56] and can be due to the exposure to environmental pollution [57], even though cases of epsomite formation on pure calcium carbonate substrates are attested if alternative sources of magnesium and/or sulphate are present [58]. In our case, the calcium sulphation due to the water infiltration that affected the considered section of South aisle wall of Monreale Cathedral could be the cause of the appearance of gypsum. The latter would probably react in turn

Fig. 8 XRD diffraction patterns of mortar and salts. **a)** mortar sample, where cal = calcite, mgs = magnesite, gp = gypsum, qz = quartz, dol = dolomite and tbn = tobermorite. **b)** salts sample, where esm = epsomite, hhy = hexahydrate and gp = gypsum. Abbreviations according to [59]



with the magnesium carbonate phases in the mortar (i.e. magnesite and dolomite), giving rise to the hydrated magnesium sulphates as end products.

4 Conclusions

These results add to the limited data available on this incredible heritage site and in general on mosaic glass after the twelfth century.

The combination of Raman spectroscopy and X-ray fluorescence analyses proved once again extremely helpful in unravelling multiple aspects of the glass composition and of its manufacture, in a fully non-destructive way. The colourless glass *tesserae* appear different from the coloured ones, which in turn are similar notwithstanding the colour. The only exception is represented by F3, which is from the figurative scene and that has some similarities with the gilded *tesserae* F1 and F2. Chromophores were successfully identified. Opacification is achieved by the use of quartz, while neither tin and/or antimony and related compounds are observed. Wollastonite has also been identified, but its origin could not be clarified from non-destructive analyses. Raman spectroscopy, moreover, seems to be able to track the specific manufacturing process of the gilded *tesserae*, requiring multiple heating steps which affect the glassy structure. Furthermore, the investigation of the bedding mortar and of the efflorescences that affect their conservation highlighted the presence of magnesium-bearing minerals in the former, with the consequent formation of hydrated magnesium sulphates as degradation products.

Supplementary Information The online version contains supplementary material available at <https://doi.org/10.1140/epjp/s13360-023-04074-2>.

Acknowledgements This research is supported by Advanced Green Materials for Cultural Heritage (AGM for CuHe) (PNR fund with code: ARS01_00697; CUP E66C18000380005), Attraction and International Mobility (AIM1833071; CUP E66C18001310007) and PON REACT (CUP E65F21002200005) projects.

Funding Open access funding provided by Università degli Studi di Catania within the CRUI-CARE Agreement. This research is supported by Advanced Green Materials for Cultural Heritage (AGM for CuHe) (PNR fund with code: ARS01_00697; CUP E66C18000380005), Attraction and International Mobility (AIM1833071; CUP E66C18001310007) and PON REACT (CUP E65F21002200005) projects. The Department of Mineral Sciences, Smithsonian Institution, is thanked for providing NMNM 117,218–1, NMNM 117,218–3 and NMNM 117,218–4 glass specimens.

Data Availability Statement This manuscript has associated data in a data repository. [Authors' comment: The datasets generated during and/or analysed during the current study are available from the corresponding author on reasonable request.]

Declarations

Conflict of interest The authors have no competing interests to declare that are relevant to the content of this article.

Open Access This article is licensed under a Creative Commons Attribution 4.0 International License, which permits use, sharing, adaptation, distribution and reproduction in any medium or format, as long as you give appropriate credit to the original author(s) and the source, provide a link to the Creative Commons licence, and indicate if changes were made. The images or other third party material in this article are included in the article's Creative Commons licence, unless indicated otherwise in a credit line to the material. If material is not included in the article's Creative Commons licence and your intended use is not permitted by statutory regulation or exceeds the permitted use, you will need to obtain permission directly from the copyright holder. To view a copy of this licence, visit <http://creativecommons.org/licenses/by/4.0/>.

References

1. M. Verità, S. Rapisarda, Riv. Della Stn. Sper. Del Vetro **2**, 15 (2008)
2. R. Arletti, M.C. Dalconi, S. Quartieri, M. Triscari, G. Vezzalini, Appl. Phys. A Mater. Sci. Process. **83**, 239 (2006)
3. E. Basso, C. Invernizzi, M. Malagodi, M.F. La Russa, D. Bersani, P.P. Lottici, J. Raman Spectrosc. **45**, 238 (2014)
4. M.-A. Gómez-Morón, T. Palomar, L. Cerqueira Alves, P. Ortiz, M. Vilarigues, N. Schibille, J. Archaeol. Sci. **129**, 105370 (2021)
5. P. Ricciardi, P. Colomban, A. Tournié, M. Macchiarola, N. Ayed, J. Archaeol. Sci. **36**, 2551 (2004)
6. A. Silvestri, S. Tonietto, G. Molin, P. Guerriero, J. Archaeol. Sci. **42**, 51 (2014)
7. I. van der Werf, A. Mangone, L.C. Giannossa, A. Traini, R. Laviano, A. Coralini, L. Sabbatini, J. Archaeol. Sci. **36**, 2625 (2009)
8. S. Murcia-Mascarós, J. Cult. Herit. **9**, 2 (2008)
9. D. Bersani, L. Saviane, A. Morigi, L. Mantovani, M. Aceto, L. Fornasini, J. Raman Spectrosc. **52**, 2234 (2021)
10. P. Ricciardi, P. Colomban, A. Tournié, M. Macchiarola, N. Ayed, J. Archaeol. Sci. **36**, 2551 (2009)
11. A. Silvestri, S. Tonietto, G. Molin, J. Archaeol. Sci. **38**, 3402 (2011)
12. A. Silvestri, S. Tonietto, F.D. Acapito, G. Molin, J. Cult. Herit. **13**, 137 (2012)
13. A. Silvestri, S. Tonietto, G. Molin, P. Guerriero, D. Geoscienze, U. Padova, V. Gradenigo, B. Culturali, U. Padova, P. Capitaniato, C.S. Uniti, J. Archaeol. Sci. **39**, 2177 (2012)
14. M.A. Gómez-Morón, T. Palomar, L.C. Alves, P. Ortiz, M. Vilarigues, N. Schibille, J. Archaeol. Sci. **129**, 105370 (2021)
15. M. Verità, A. Renier, S. Zecchin, J. Cult. Herit. **3**, 261 (2002)
16. M. Verità, in *Sci. e Tec. Del Restauro Della Basilica Di San Marco*, edited by E. Vio (Istituto Veneto di Scienze, Lettere ed Arti, Venice, Italy, 1999), pp. 567–585.
17. B. Dal Bianco, U. Russo, J. Non. Cryst. Solids **358**, 368 (2012)
18. C. Boschetti, A. Corradi, P. Baraldi, J. Raman Spectrosc. **39**, 1085 (2008)
19. F. Izzo, A. Arizzi, P. Cappelletti, G. Cultrone, A. De Bonis, C. Germinario, S.F. Graziano, C. Grifa, V. Guarino, M. Mercurio, V. Morra, A. Langella, Constr. Build. Mater. **117**, 129 (2016)
20. A. Fragata, J. Ribeiro, C. Candeias, A. Velosa, F. Rocha, Appl. Sci. **11**, 8267 (2021)
21. M.L.S. Oliveira, B.F. Tutikian, C. Milanes, L.F.O. Silva, J. Clean. Prod. **248**, 119250 (2020)
22. C. Fiori, M. Vandini, S. Prati, G. Chiavari, J. Cult. Herit. **10**, 248 (2009)
23. M.F. Alberghina, A. Casanova Municchia, G. Germinario, A. Macchia, M. Matteini, G. Milazzo, S. Ruffolo, L. Sabbatini, S. Schiavone, A. Sodo, M. Ricca, M.F. La Russa, Int. J. Conserv. Sci. **11**, 353 (2020)
24. M. Fugazzotto, R. Occhipinti, M. Cristina Caggiani, A. Coccato, C. Finocchiaro, G. Lanzafame, P. Mazzoleni, G. Nucatolo, G. Piacenti, S. Starinieri, A. Strosio, G. Barone, Mater. Lett. **333**, 133626 (2023)
25. G. Barone, M. C. Caggiani, A. Coccato, C. Finocchiaro, M. Fugazzotto, G. Lanzafame, R. Occhipinti, A. Strosio, and P. Mazzoleni, in *IOP Conf. Ser. Mater. Sci. Eng.* (Institute of Physics Publishing, 2020), p. 012001.
26. F. Koleini, P. Colomban, A. Antonites, I. Pikirayi, J. Archaeol. Sci. Reports **13**, 333 (2017)
27. F. Koleini, L.H. Machiridza, I. Pikirayi, P. Colomban, Archaeometry **61**, 874 (2019)
28. I.M.N. Ribeiro, R.P. Freitas, C. Calza, A.L.C. Oliveira, V.S. Felix, D.S. Ferreira, R.T. Batista, E.A.S. Gonçalves, M.O. Pereira, P.C.L. Brito, T.A. Lima, A.R. Pimenta, M.J. Anjos, R.T. Lopes, Vib. Spectrosc. **87**, 111 (2016)
29. A. Coccato, M. Costa, A. Rousaki, B.O. Clist, K. Karklins, K. Bostoen, A. Manhita, A. Cardoso, C. Barrocas Dias, A. Candeias, L. Moens, J. Mirão, P. Vandenabeele, J. Raman Spectrosc. **48**, 1468 (2017)
30. A. Rousaki, A. Coccato, C. Verhaeghe, B.-O. Clist, K. Bostoen, P. Vandenabeele, L. Moens, Appl. Spectrosc. **70**, 76 (2016)
31. L.W. Adlington, Pap. from Inst. Archaeol. **27**, 1 (2017)
32. P. Colomban, J. Non. Cryst. Solids **323**, 180 (2003)
33. A. Cesaratto, P. Sichel, D. Bersani, P.P. Lottici, A. Montenero, E. Salvioli-Mariani, M. Catarsi, J. Raman Spectrosc. **41**, 1682 (2010)
34. V.A. Solé, E. Papillon, M. Cotte, P. Walter, J. Susini, Spectrochim. Acta - Part B At. Spectrosc. **62**, 63 (2007)
35. L.W. Adlington, I.C. Freestone, MRS Adv. **357**, 1 (2017)
36. P. Colomban, A. Tournié, M.C. Caggiani, C. Paris, J. Raman Spectrosc. **43**, 1975 (2012)
37. L. Robinet, C. Coupry, K. Eremin, C. Hall, J. Raman Spectrosc. **37**, 789 (2006)
38. P. McMillan, Am. Mineral. **69**, 622 (1984)
39. C.T. Ho, W.C. LaCourse, R.A. Condrate, A. Jillavenkatesa, Mater. Lett. **23**, 237 (1995)
40. P. Colomban, A. Tournié, L. Bellot-Gurlet, J. Raman Spectrosc. **37**, 841 (2006)
41. I.C. Freestone, Geol. Soc. Spec. Publ. **257**, 201 (2006)
42. K.H. Wedepohl, A. Baumann, Naturwissenschaften **87**, 129 (2000)
43. S. Maltoni, A. Silvestri, J. Cult. Herit. **39**, 251 (2019)
44. A. Silvestri, G. Molin, G. Salviulo, J. Non Cryst. Solids **351**, 1338 (2005)
45. R. Arletti, S. Quartieri, G. Vezzalini, G. Sabatino, M. Triscari, M.A. Mastelloni, J. Non. Cryst. Solids **354**, 4962 (2008)
46. A. Silvestri, F. Nestola, L. Peruzzo, Microchem. J. **124**, 811 (2016)
47. P. Colomban, G. Sagon, X. Faurel, J. Raman Spectrosc. **32**, 351 (2001)

48. M.C. Caggiani, G. Barone, L. de Ferri, R. Laviano, A. Mangone, P. Mazzoleni, J. Raman Spectrosc. **52**, 186 (2021)
49. A. Iyiel, D. Oktem, F. Akmaz, J. Chem. Chem. Eng. **8**, 849 (2014)
50. S. Rossano, V. Khomenko, A. Bedidi, C. Muller, C. Loisel, J. Ferrand, L. Sarrasin, A. Bertin, J. Non. Cryst. Solids **594**, 121710 (2022)
51. M. Verità, in *Mediev. Mosaic; Light. Color. Mater.* (Silvana Editoriale, Milan, 2000), pp. 47–64.
52. L. Borromeo, U. Zimmermann, S. Andò, G. Coletti, D. Bersani, D. Basso, P. Gentile, B. Schulz, E. Garzanti, J. Raman Spectrosc. **48**, 983 (2017)
53. B. Lafuente, R.T. Downs, H. Yang, N. Stone, in *Highlights Mineral. Crystallogr.* ed. by T. Armbruster, R.M. Danisi (W. De Gruyter, Berlin, 2015), pp.1–30
54. N. Prieto-Taboada, O. Gómez-Laserna, I. Martínez-Arkarazo, M.Á. Olazabal, J.M. Madariaga, Anal. Chem. **86**, 10131 (2014)
55. A. Wang, J.J. Freeman, B.L. Jolliff, I.M. Chou, Geochim. Cosmochim. Acta **70**, 6118 (2006)
56. P. Lopez-Arce, J. Garcia-Guinea, D. Benavente, L. Tormo, E. Doehne, Constr. Build. Mater. **23**, 846 (2009)
57. H. Siedel, Environ. Earth Sci. **69**, 1249 (2013)
58. S. Eric, V. Matovic, A. Kremenovic, P. Colombar, D. Sreckovic Batocanin, M. Neškovic, A. Jelkic, D. Srec, Constr. Build. Mater. **98**, 25 (2015)
59. L.N. Warr, Mineral. Mag. **85**, 291 (2021)